

RESEARCH ARTICLE

Hypertonic external medium represses cellular respiration and promotes Warburg/Crabtree effect

Minoo Hamraz¹ | Raymond Abolhassani² | Mireille Andriamihaja³ | Céline Ransy¹ |
 Véronique Lenoir¹ | Laurent Schwartz⁴ | Frédéric Bouillaud¹

¹Institut Cochin, INSERM, CNRS, Université de Paris, Paris, France

²SAS Vaccinopole, Paris, France

³INRA/AgroParisTech UMR 914, Physiologie de la Nutrition et du Comportement Alimentaire, Paris, France

⁴Assistance Publique des Hôpitaux de Paris, Paris, France

Correspondence

Frédéric Bouillaud, Institut Cochin, INSERM, CNRS, Université de Paris, 75014 Paris, France.

Email: frederic.bouillaud@inserm.fr

Funding information

Institut National de la Santé et de la Recherche Médicale (Inserm); Centre National de la Recherche Scientifique (CNRS); Université Paris Descartes (Paris Descartes University)

Abstract

Hyperosmotic conditions are associated to several pathological states. In this article, we evaluate the consequence of hyperosmotic medium on cellular energy metabolism. We demonstrate that exposure of cells to hyperosmotic conditions immediately reduces the mitochondrial oxidative phosphorylation rate. This causes an increase in glycolysis, which represses further respiration. This is known as the Warburg or Crabtree effect. In addition to aerobic glycolysis, we observed two other cellular responses that would help to preserve cellular ATP level and viability: A reduction in the cellular ATP turnover rate and a partial mitochondrial uncoupling which is expected to enhance ATP production by Krebs cycle. The latter is likely to constitute another metabolic adaptation to compensate for deficient oxidative phosphorylation that, importantly, is not dependent on glucose.

KEYWORDS

bioenergetics, cancer, Crabtree effect, inflammation, Krebs cycle, Warburg effect

1 | INTRODUCTION

1.1 | Hyperosmolarity, inflammation, and cancer

The hyperosmotic status is physiological in the kidney but elsewhere the pathological consequences of hyperosmolarity may have been overlooked.¹ Hyperosmolarity has been reported in several inflammatory diseases. These include Crohn's disease and ulcerative colitis,² as well as the inflammatory bowel disease (IBD) of the newborn and

neonatal necrotizing enterocolitis³ or inflammatory pleural effusion.⁴ The increase in the capillary permeability is an early step of the inflammation process that causes protein extravasation and their subsequent hydrolysis into osmotically active amino acids and peptides. This is aggravated by cell death and additional hydrolysis of macromolecules. Hence, the extracellular medium becomes hypertonic at the inflammatory site. Finally, hyperosmolarity has also been measured in tumors⁵⁻⁷ where it is thought to prevent the delivery on target of antineoplastic drugs.⁸

Abbreviations: BCA, bichoninic acid; CCCP, carbonyl cyanide m-chlorophenyl hydrazine an uncoupler of mitochondrial respiration; DMEM, Dulbecco's modified Eagle medium; ETS, electron transfer system: estimation of the maximal activity of mitochondrial redox complexes (I-IV) as obtained by measurement of oxygen consumption rate in the presence of optimal concentration of uncoupler; LDH, lactate dehydrogenase; OCR, oxygen consumption rate; OxPhos, mitochondrial oxidative phosphorylation (action of mitochondrial complexes I-V); PPR, proton production rate.

1.2 | Cellular bioenergetics

At the level of the whole organism, the energy needs of mammals are ultimately met by oxidative metabolism, which includes CO₂ release and mitochondrial oxygen (O₂) consumption coupled to ATP production. However, at the cellular level, lactic fermentation might become an important contributor for ATP production. This lactic fermentation is the conversion of one molecule of glucose into two molecules of lactate (final product) with formation of two ATP and no oxygen consumption. The term “glycolysis” will be used here as opposed to the terms respiration or oxidative phosphorylation (OxPhos). At this point, it is important to remember that in the absence of ATP regeneration the cellular ATP concentration would be exhausted within dozens of seconds and ATP depletion will result in cell death. Hence, when minutes/hours of cellular life are to be considered (this study), the ATP consumption rate and the ATP production rate are matched and modifications in these fluxes reflect either a change in cellular ATP turnover rate and/or differences in the relative contributions of respiration and glycolysis. Manipulation of substrates in the extracellular medium and addition of mitochondrial poisons or uncouplers allow the evaluation of which steps are involved.⁹ The balance between respiration and glycolysis and their crosstalk is a long-standing issue in metabolic studies and two fields of research illustrate its importance: cancer, since the formulation of “Warburg hypothesis”,^{8,10-14} and inflammation.¹⁵⁻¹⁷ The present study aims to evaluate the consequences of hyperosmotic stress on cellular energy metabolism and bioenergetics. Our results demonstrate that modifications of cellular energy metabolism are detectable almost immediately after an increase in osmolarity. This response is shared between different cell types and different osmolytes and can be observed at either 450 or 600 mOsm/L.

2 | MATERIALS AND METHODS

2.1 | Reagents and equipment

Mannitol (M4125), glucose (G6152), galactose (G5388), oligomycin (O4876), antimycin A (A8674), carbonyl cyanide *m*-chlorophenyl hydrazone (CCCP C2759), KCN (60178), rotenone (R8875), ADP (A4386), ATP (A7699), succinic acid (S5049), glutamic acid (G1626), malic acid (M7397), digitonine (D5628), glacial acetic acid (A-6283), and polyethylene glycol 400 (P-3265) were obtained from Sigma-Aldrich (St Louis MO-USA), ethanol 96% (CARLO ERBA Val de Reuil-France), sodium pyruvate 100 mM from GIBCO Life Technologies (Carlsbad CA-USA), NAD (free acid, grade I, ref. 10127965001), and lactate dehydrogenase (ref. 10127230001) from Roche (Mannheim-Germany). Seahorse

XF Assay Medium (102365-100) was obtained from Agilent (Santa Clara CA-USA).

Quantitation of extracellular fluxes (oxygen consumption, acid release) used the “Seahorse” extracellular flux analyzer XF96 (Seahorse Bioscience, North Billerica MA-USA). High-resolution respirometry was performed with the oxygraph O2k (Oroboros Instruments, Innsbruck-Austria). Measurements in 96-well plates and absorbance readings used a microtiter plate reader spectrophotometer (TECAN Infinite 200M, Männedorf-Switzerland).

2.2 | Cell culture

All cultures were incubated at 37°C in a humidified incubator with 5% CO₂. CHO cells were cultured in F-12 Nutrient Mix (1X) GlutaMax (HAM) supplemented with 10% (v/v) inactivated fetal bovine serum (FBS), 50 U/mL penicillin, and 50 µg/mL streptomycin (all from GIBCO, Life Technologies). This study used CHO-K1 and a subclone (CHO-CO3) obtained after transfection with pcDNA3 empty vector and selection for geneticin resistance (Lagoutte 2010) with passage number 8-17. Other cell lines were cultured in Dulbecco's modified Eagle's medium high-glucose (DMEM, Life Technologies Carlsbad CA-USA) supplemented with 10% (v/v) inactivated fetal bovine serum (FBS), 50 U/mL penicillin, and 50 µg/mL streptomycin. The human neuroblastoma cell line SH-SY5Y was obtained from ATCC (American Type Culture Collection, Manassas VA-USA) batch number 63990073 and used from passage 8 to 12. The subclone HT-29 Glc ^{-/+} selected for growth and differentiation in the absence of glucose¹⁸ was used with passage from 44 to 48. Human embryonic Kidney HEK-293 culture was obtained from another team in the same institute (passage number 9-12). The morphology of these different cell lines was checked during the growing procedure and remained well in line with the pictures available from ATCC. Moreover, different respiratory rates appear as a further distinctive trait of different cell lines (see results).

2.3 | Measurement of oxygen consumption

For measurement in the oxygraph O2k, the cells were harvested using trypsin and resuspended in their respective growing medium. The density of the cellular suspension was estimated from optical density at 600 nm using a calibration curve established for the different cell lines between cell counting (cytometry) and optical density. Two ml of a suspension of cells ($1-2 \times 10^6$ cells/mL) was placed in each of the two chambers of the oxygraph, and allowed to equilibrate for 5 minutes before closure of the chambers to start respiration rate measurement. After recording of the basal rate of

oxygen consumption, the chambers were opened and osmotic stress was triggered by adding solid mannitol to one of the chambers to increase osmolarity with minimal disturbance in final volume/composition. Cells were challenged with two different final concentrations of mannitol: 150 or 300 mM (450 or 600 mOsm/L final osmolarity).

Inhibitors and uncouplers were used to provide information on the mechanisms underlying cellular oxygen consumption. The extent of oxygen consumption explained by mitochondrial oxidative phosphorylation (ATP production) was deduced from the inhibition of oxygen consumption rate (OCR) caused by oligomycin (1 μ M final), an inhibitor of the mitochondrial complex V (FoF1 ATP synthase). An optimal concentration (0.5–7 μ M) of the uncoupler, CCCP, increased OCR to a maximal value thought to represent the maximal possible recruitment of mitochondrial respiratory enzymes. Finally, the addition of the complex III inhibitor (antimycin 4.5 μ M final) abolished oxygen consumption due to mitochondrial respiratory chain and the remaining oxygen consumption represents other (non-mitochondrial) oxygen consumption processes.

The difference (oligomycin-OCR minus antimycin-OCR) represents the activity of the mitochondrial respiratory chain that is explained by processes other than ATP turnover rate, namely proton leakage across inner membrane and, therefore, the term “Leak” is used. The difference between the maximal OCR in the presence of CCCP and antimycin-OCR indicates the maximal activity for the mitochondrial electron transfer system (ETS). Actually, this ETS rate reflects the maximal rate for the metabolic pathway starting with substrate entry, followed by oxidation into CO₂, and ending by electron transfer and oxygen consumption at the level of mitochondrial respiratory chain (mitochondrial respiratory complexes I–IV). The OCR was expressed with regard to the number of cells in pmol O₂/(second \times million cells).

2.4 | Extracellular flux measurements

CHO cells were inoculated at 30 000 cells per well in XF96-plate in normal medium (F12) for 8 hours to attach. Before running the experiment, the growth medium was replaced with warmed DMEM XF medium (HCO₃-free modified DMEM, Seahorse Bioscience with pH set to 7.4) which contained: (i) glucose (10 mM glucose, 1 mM pyruvate), (ii) glucose free (1 mM pyruvate), or (iii) galactose (10 mM galactose, 1 mM pyruvate) and incubated for 30–60 minutes at 37°C in air. HT29 cells were inoculated at 30 000 cells per well in XF96-plate in normal medium (DMEM high glucose) for 12 hours to attach. Before running the experiment, the growth medium was removed replaced by warmed DMEM XF medium (HCO₃-free modified DMEM, Seahorse Bioscience with pH set to 7.4) which contained: (i) glucose

(25 mM glucose, 1 mM pyruvate) or (ii) glucose free (1 mM pyruvate). Hyperosmotic stress was triggered by injecting a mannitol solution in DMEM XF assay medium (700 mM mannitol, hence 1000 mOsm/L), two injection ports loaded with 45 μ L of mannitol solution were used successively to reach a final osmolarity close to 600 mOsmol/L (actually 574). Control wells were injected with the same volume of DMEM medium. To follow modifications of cellular bioenergetics with time after the osmotic challenge, several cycles of measurement (mix 4 minutes, measurement 3 minutes) were performed with increasing (3, 13, and 23 minutes) time delay between them. Usually 12 wells were utilized for each single group (same metabolic and osmotic conditions).

2.5 | Mitochondrial preparation

Rat liver mitochondria were obtained from male 5-week-old-SPF Wistar rats (Janvier Labs 53940 Le Genest St Isle France). Animals were sacrificed following national and local guidelines (Authorization number B75-14-02) and 3–4 g of liver tissue were homogenized in the mitochondrial preparation buffer (300 mM sucrose, 5 mM tris base, 1 mM EGTA, pH 7.4). Mitochondria were prepared by differential centrifugation. The final mitochondrial pellet was resuspended in the same buffer (50–100 mg protein/ml final concentration). Protein concentration was obtained by the BCA method with bovine serum albumin (BSA) as a standard. For measurement of oxygen consumption, mitochondria were resuspended in mitochondrial respiration buffer (KCl 100 mM, Sucrose 40 mM, TES 10 mM, MgCl₂ + 6H₂O 5 mM, EGTA 1 mM, BSA 0.4%, K-Pi 20 mM) at 0.5 mg protein/ml final; measurements were made at 25°C. In this medium, the sucrose could be replaced by glucose. Mitochondrial respiration was initiated by addition of the substrates glutamate/malate (5 mM final concentration), then ADP (1.25 mM final concentration) was added to stimulate respiration and evaluate the respiratory control ratio (RCR); (oxygen consumption in presence of substrate and ADP)/(oxygen consumption in absence of ADP, or in the presence of oligomycin). The RCR for a fresh preparation should be between 15 and 20; the preparation was discarded if the RCR fell below 10. Because of this high RCR, these mitochondrial preparations retain a viable coupling state when stored overnight at 0°C (5 < RCR < 15) and could be used the following day. Hypertonic conditions were obtained by doubling the concentration of the respiration buffer to maintain the composition of the respiring medium. Alternatively, similar to cell studies, hypertonic conditions were obtained by addition of 300 mM mannitol to the 1X mitochondrial respiration buffer. Experiments were paired with one chamber of the oxygraph O2k used as the reference “isotonic control” to which the same other additions (substrate, ADP, poisons) were made.

2.6 | Cytotoxicity

CHO cell viability was assessed colorimetrically by the neutral red uptake method¹⁹ using neutral red stock solution 4 mg/mL and neutral red destaining solution (50% ethanol 96%, 49% deionized water, 1% glacial acetic acid). The uptake of neutral red depends on the cell's capacity to maintain pH gradients, through the production of ATP. CHO cells were inoculated at 5000 cells per well in 96 microplate in normal medium (F12) and left for 12 hours (37°C 5% CO₂) to attach. Then growth medium was replaced by warmed DMEM XF medium (HCO₃-free modified DMEM, Seahorse Bioscience with pH set to 7.4) in "glucose" (10 mM glucose, 1 mM pyruvate) or "glucose free" (1 mM pyruvate) conditions. Cells were exposed to 600 mOsm (mannitol) or 300 mOsm/L (control) for 2, 4, 6, and 8 hours at 37°C in room air, the medium was removed and 100 μ L of neutral red (diluted 1:100 in cell culture medium) was added to each well followed by 4 hours of incubation. The neutral red medium was removed and the cells were washed two times with 150 μ L PBS and 150 μ L of neutral red destaining solution was added. The microplates were shaken gently for 30 minutes in room temperature and the absorbance was read at 540 nm.

2.7 | Data treatment and statistical analysis

Data were analyzed with GraphPad Prism 7.04 (GraphPad Software La Jolla CA 92037 USA) or Microsoft Excel (Microsoft Corporation Redmond 98052 WA USA). Unless specified, the non-parametric test (Mann-Whitney) was used to assess statistical significance with $P < .05$, of at least three independent experiments; data are shown as mean values \pm SD.

3 | RESULTS

3.1 | Hyperosmotic conditions impact on cellular oxygen consumption

When respiring CHO cells were subject to an osmotic shock (abrupt increase in osmotic pressure), oxygen consumption rate (OCR) decreased within few minutes to a new lower value (Figure 1A). This inhibition persisted for hours when the medium osmolarity was doubled (Figure 1 black dots/histograms). A milder osmotic challenge (50% increase in osmolarity to 450 mOsm/L) caused the same initial oxygen consumption decrease but it appeared at least partially reversible with time (Figure 1 grey dots/histograms). This depression of cellular OCR after osmotic shock was verified with three other cell lines (compare "basal" versus "basal before" in Figure 2). Moreover, a similar effect was found with two

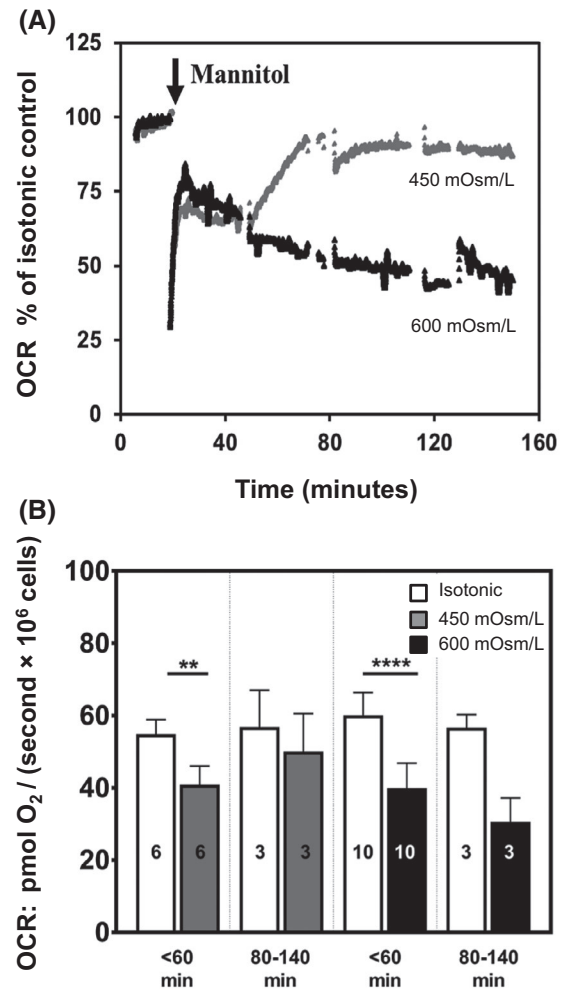


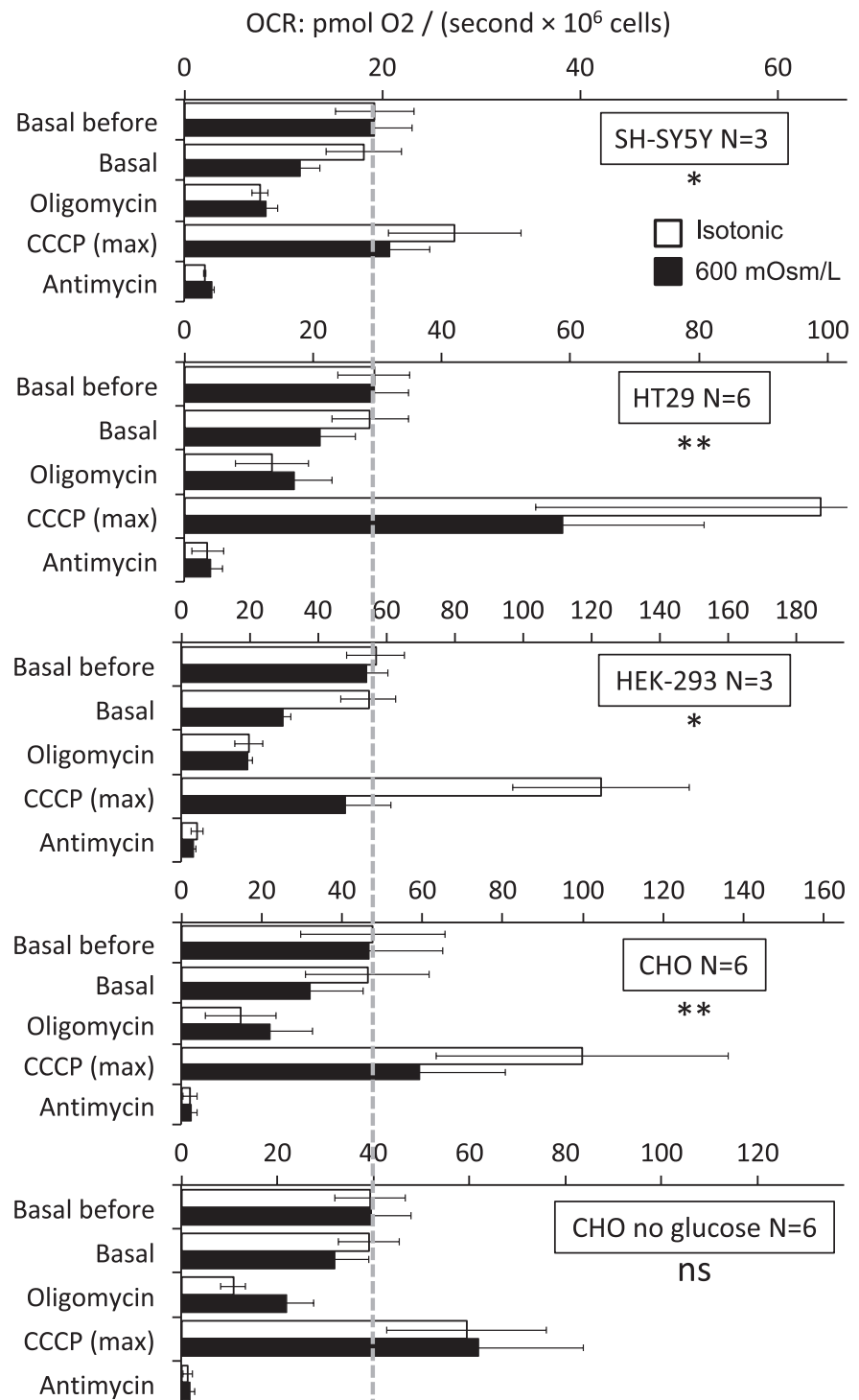
FIGURE 1 Oxygen consumption rates of CHO cells in hyperosmotic conditions. A, Representative experiments with CHO cells ($1-2 \times 10^6$ cells/mL in 2 ml of medium with 10 mM glucose), X-axis: time (minutes), the arrow indicates the time of mannitol dissolution in one of the two chambers of the O₂k oxygraph, grey dots: 150 mM (450 mOsm/L final) and black dots 300 mM (600 mOsm/L final). The other chamber is used to record oxygen consumption rate of the isotonic control. The Y-axis is the cellular oxygen consumption rate (OCR) expressed as the ratio (in %) with the control for each time point (every 2 seconds). The sharp decrease immediately after mannitol addition was coincident with a peak in the activity of the Peltier element maintaining the temperature of the measurement chambers. It is likely to reflect the compensation for a transient period of heat consumption caused by mannitol dissolution expected to impact transiently on temperature hence cellular oxygen consumption. The interruptions in the graph reflect re-oxygenation steps with opening and closure of the chambers generating extreme negative OCRs not shown here for the sake of clarity. B, Mean values for cellular oxygen consumption rate expressed in pmoles O₂/(second \times 10⁶ cells) in the short term after mannitol addition (<60 minutes) and in the mid-term (80-140 minutes): control isotonic condition 300 mOsm/L (white), 450 mOsm/L (150 mM mannitol) grey, 600 mOsm/L (300 mM mannitol) black. Figures on bars refer to the number of independent experiments, when the differences reached statistical significance this is indicated with ** $P < .01$ and **** $P < .0001$

other osmolytes: polyethylene glycol and sodium chloride (Supplemental Figure S1).

Cellular oxygen consumption is to a large extent explained by mitochondrial respiration, which can be investigated further with the help of molecules that impact on specific steps of the mitochondrial oxidative phosphorylation process (Supplemental Figure S2). When the OCR was expressed in absolute values (pmol O₂/(second × million cells)), different

values were obtained with the different cell lines (Figure 2, Supplemental Figure S3). However, when expressed with reference to an internal reference rate (the basal rate before the osmotic challenge in the same experiment), the relative responses of the different cell lines were similar and errors bars were greatly reduced (Supplemental Figure S3). Computation of these different rates allowed a quantitative analysis of the different processes explaining the basal cellular OCR. A part

FIGURE 2 Cellular mitochondrial bioenergetics. The OCR in pmol O₂/(second × 10⁶ cells) was determined over the same period for both chambers of the oxygraph O2k. In one chamber (white bars), cells were kept in their isotonic medium, in the other chamber mannitol 300 mM final (600 mOsm/L) was added (black bars). The basal OCR in both chambers before mannitol addition is shown and scales have been adjusted for alignment of initial basal respiratory rates (vertical dotted grey line) allowing comparison of relative variations caused by inhibitors (oligomycin, antimycin) and uncoupler (CCCP). All rates were obtained within about 1 hour after the osmotic shock. Below the indication of the cell line is shown the statistical significance for the comparison between isotonic and hypertonic for the fast rates (basal and CCCP (max)) using the Wilcoxon signed-ranked test (Vassarstats.net) **P* ≤ .05 ***P* < .01. Supplemental Figures S3 and S4 represent the same data after their normalization using an internal reference rate



is caused by non-mitochondrial oxygen consumption for which the OCR observed in presence of antimycin provided a direct estimation. This non-mitochondrial OCR was always low and not different between isotonic and hypertonic conditions (Figure 2). Mitochondrial basal oxygen consumption (Mitoch. basal) reflects the sum of oxidative phosphorylation (OxPhos) and energy loss (Leak). Finally, the maximal possible activity of the mitochondrial electron transfer system (ETS) could be estimated from the maximal CCCP rate. The relative effect of hyperosmolarity differed significantly for these different processes (Figure 3). The most dramatic change was a severe decrease in OxPhos to about 30% of isotonic control. In contrast, the leak appeared either unchanged

or increased (ratio equal or higher than 1). The consequence is that OxPhos accounted for 70% of the basal OCR in isotonic conditions and only 30% of the basal OCR observed under hypertonic conditions (Supplemental Figure S4). The ETS rate was affected as well, but to a lesser extent than the OxPhos (Figure 3). Notably, with CHO cells, in absence of glucose the ETS was not affected by hypertonic conditions (ratio equals 1 in Figure 3). The preservation of the ETS rate for the cell suspension ruled out cellular disruption caused by addition and dissolution of mannitol, which would dilute metabolic intermediates, enzymes, and redox cofactors and was then expected to impact largely on the ETS rate.

A possible explanation would be a direct impact of hyperosmotic conditions on mitochondrial bioenergetics. To examine this hypothesis, we evaluated the impact of a hypertonic respiration medium on the respiration of isolated liver mitochondria (Figure 4). We could not record any adverse effect of the hypertonic medium (Figure 4A,B). In the experiment shown, the effect of the hyperosmotic medium on mitochondrial volume could be seen by the difference in optical density of the mitochondrial suspension (Figure 4A lines and right scale). A difference with experiments made with cells was the presence of saturating amounts of substrate and ADP (state 3) that ensured the fastest possible ADP phosphorylation rate with oxygen consumption close enough to maximal uncoupled rate (CCCP, Figure 4C). Consequently, the calculated oxygen consumption rates for ATP production and ETS were similar. The higher hyperosmotic CCCP (ETS) rate was statistically significant (Figure 4C,D). This measurement was made late in the experiment and the difference is likely the result of better preservation of mitochondrial function in hypertonic buffer (Guedouari & Bouillaud unpublished results). This is supported by the continuous decrease in stimulated rates for isotonic control (grey trace in Figure 4A). The small increase observed after addition of oligomycin (state 4) reached significance when the Leak rate was calculated (Figure 4D).

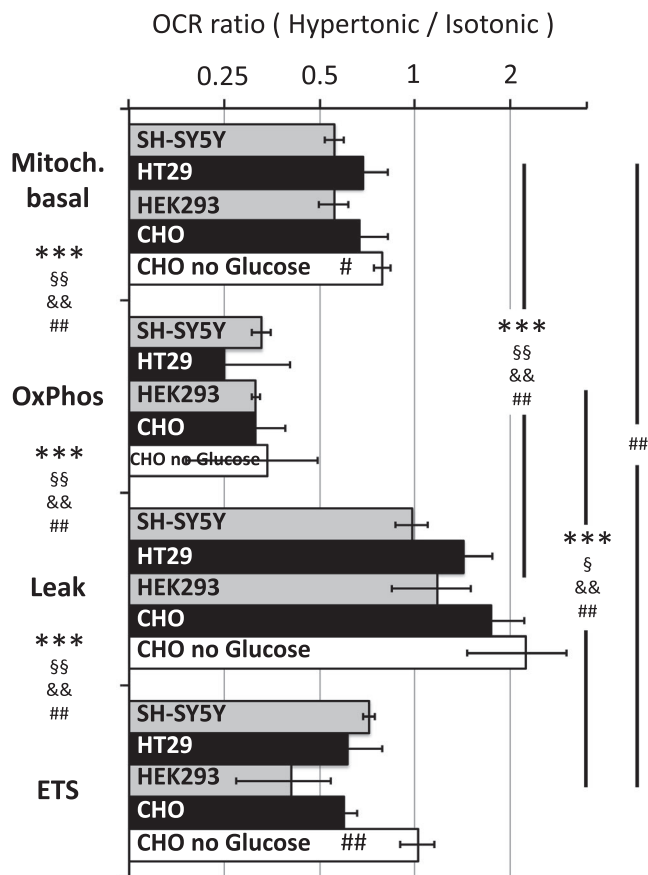


FIGURE 3 Relative impact of hyperosmolarity. Original data are those shown in Figure 2. The different rates basal mitochondria OCR (Mitoch. Basal), oxidative phosphorylation (OxPhos), mitochondrial leak (Mitoch. Leak), and maximal electron transfer system activity (ETS) were determined from the cellular OCR rates (see Material and Methods section) and the ratio between hyperosmotic and isosmotic values is shown here (mean \pm SD). When the differences reached statistical significance, this is indicated for all values in presence of glucose $n = 18$ (*** $P < .001$) and for HT29 $n = 6$ (§§ $P < .01$) and CHO $n = 6$ (&& $P < .05$, ## $P < .01$). The symbols (#) refer to statistical significance (# $P < .05$, ## $P < .01$) for the difference in presence/absence of glucose (CHO cells only), when on the “CHO no glucose” bar the comparison refer to the black bar just above

3.2 | OxPhos and glycolysis contribution to cellular bioenergetics

The contribution of mitochondrial respiration and of glycolysis to cellular ATP turnover could be evaluated simultaneously with the extracellular flux analyzer (Seahorse). Moreover, since the cells are attached, the experiment can be followed over the long term. As described above, experiments included the measurement of basal cellular OCR and extracellular acidification rate before hypertonic conditions were imposed. OCR and acidification rate were then followed over 6 hours for isotonic control and hyperosmotic challenged cells in media with or without glucose (Figure 5A-D). To improve comparison of respiratory and glycolytic fluxes,

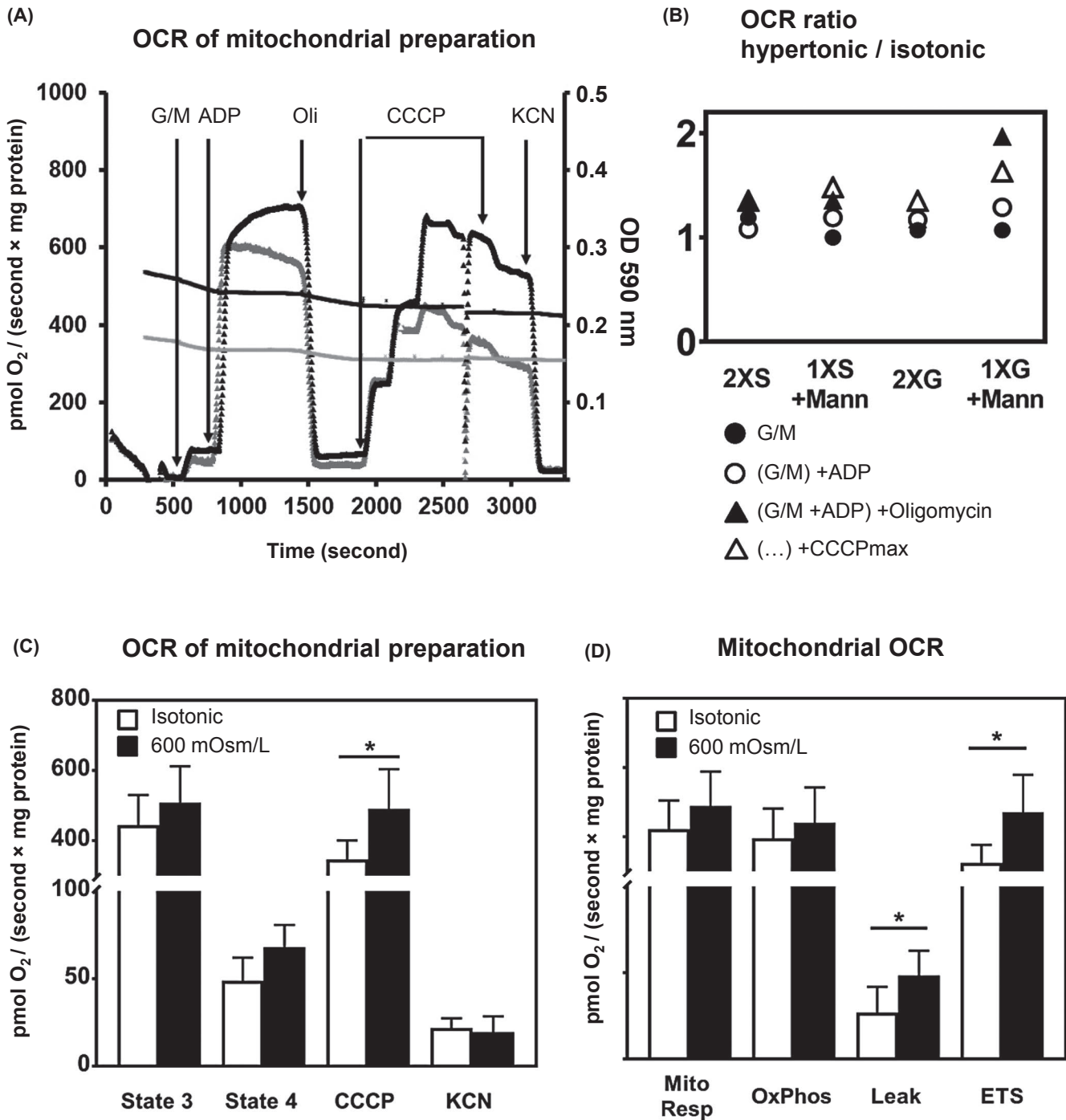


FIGURE 4 Isolated rat liver mitochondria. A, Representative experiment: dots represent the oxygen consumption rate (left scale) and lines the optical density (right scale) of the mitochondrial suspension at 590 nm obtained by adaptation of fluorescent module to report absorbance of the light of the diodes illuminating the Oxygraph chambers (C. Ransy and F. Bouillaud unpublished). Black symbols/line represent hypertonic conditions (600 mOsm/L) and grey isotonic control (300 mOsm/L). B, Ratio of hypertonic OCR/isotonic OCR: data from all experiments with isolated mitochondria in respiration media with sucrose or glucose (see M & M section). Hyperosmolar conditions were obtained either by the use of the medium concentrated two times (2X) with sucrose (2XS: mean value of three experiments) or Glucose (2XG); or 1X media plus mannitol 1XS + Mann or 1XG + Mann. The legend shows the different symbols that refer to the successive conditions for mitochondrial respiration as visible in part A. C, Mean values for OCR expressed in pmol O₂/(second × mg protein) of rat liver mitochondria under conditions as shown in A: “State 3” (phosphorylation state in the presence of substrate and 1.25 mM ADP); “State 4” after addition of oligomycin; maximal uncoupled rate (CCCP) and non-mitochondrial oxygen consumption (inhibition by cyanide KCN). Empty bars isotonic mitochondrial buffers, black bars two times hypertonic buffers (see legend to part B). D, Interpretation of these rates similarly as with cells when the difference reached statistical significance this is indicated with **P* < .05

the acidification rate was converted into proton production rate (PPR) in pmol H⁺ per minute and per well (Figure 5C,D) and the units were fully consistent with those of OCR expressed in pmol O₂ per minute and per well (Figure 5A,B). To provide a picture closer to their contribution to cellular

bioenergetics (ATP turnover rates), the proportionality between lactate release or oxygen consumption and ATP production was considered. In glycolysis, one molecule of glucose releases two molecules of lactate (two protons) and generates two ATP. Hence, PPR approximates the ATP

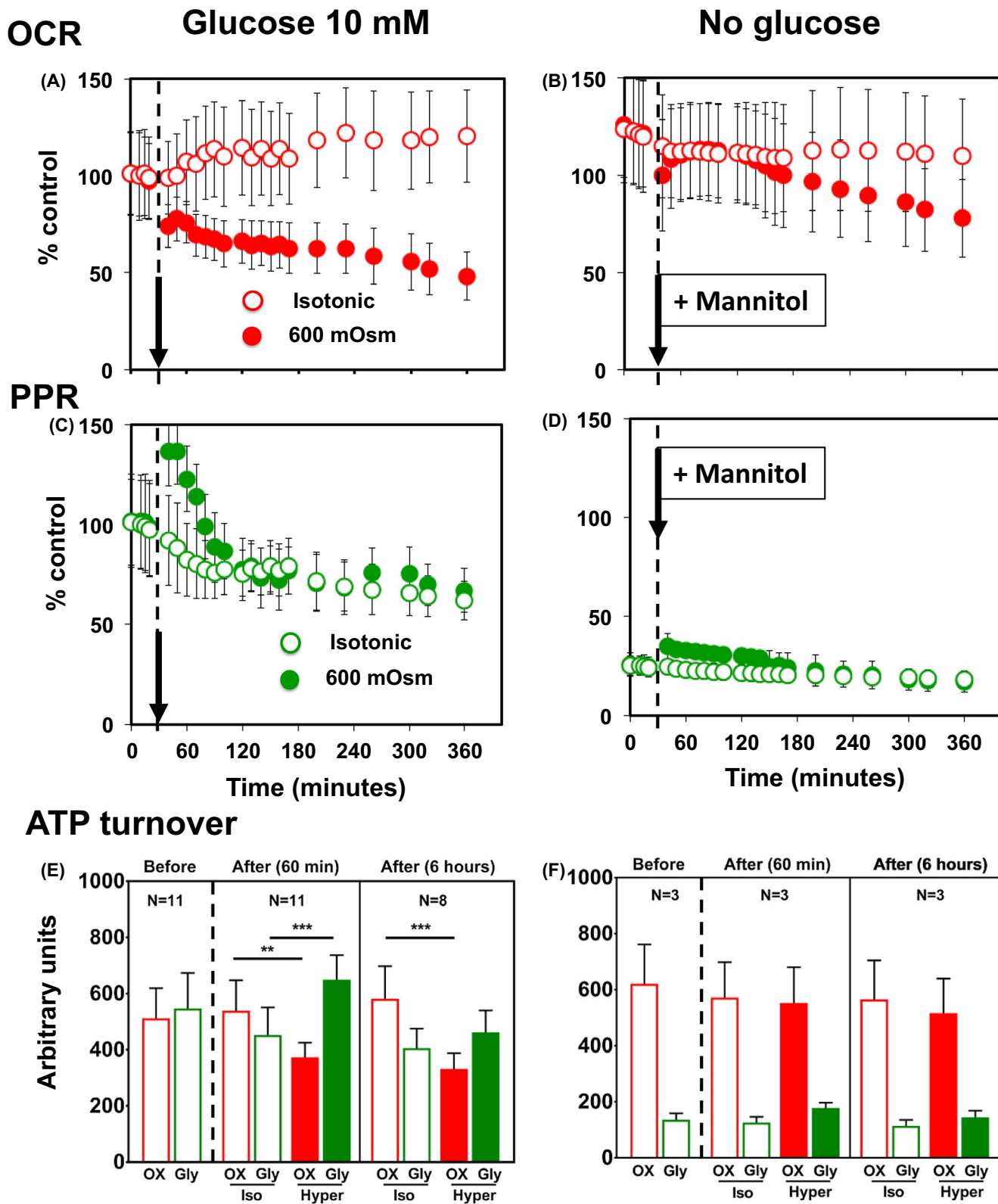


FIGURE 5 Oxygen consumption rate (OCR) and proton production rate (PPR). A-D, Seahorse measurements with CHO cells with OCR in red (A, B) and PPR in green (C, D) the X-axis is time in minutes, isotonic conditions are empty symbols and hypertonic filled symbols. In each experiment, one half of the wells were subject to osmotic shock (injection of mannitol solution) and other were treated as control (injection of solvent). The time of mannitol addition is indicated (unless it would overlap with symbols/legend) and a vertical dotted line separates the values obtained before (isotonic and hypertonic are superposed) and after it. The errors bars refer to the standard deviation of OCR or PPR values for the independent “Seahorse experiments” (number of experiments is given in E, F). Each value from a single experiment was the average of 24/12 replicates (Seahorse plate wells). Because the actual cell number in the well/under the Seahorse probe could not be accurately determined at the time of measurement the Y scale was converted to present values as the percentage of a reference rate (the mean value of the rates before the osmotic shock in presence of glucose). E, F, Histograms representation with units closer to OCR or PPR relative contribution to the ATP turnover: one lactate (PPR unit) equals one ATP and one O₂ (OCR unit) equals 5 ATP. For these calculations, the values of OCR or PPR in Seahorse units: pmoles (O₂ or H⁺)/(minute × well) were used and resulted in ATP turnover rates in pmoles ATP/(minute × well). Inaccuracy with regard to cell number (see above) means that they are to be considered as “arbitrary units.” A vertical dotted line separates the values obtained before and after mannitol addition. The color code is consistent with above. Mean values are shown in the short term: 10-60 minutes after mannitol addition or for the long term: mean value over the whole period of time of (10 minutes-6 hours after mannitol addition). Standard deviation represents therefore both variability between experiments and kinetic effect. Legend below the figure: OX: oxidative phosphorylation (5 × OCR); Gly: Glycolytic (PPR); Iso: Isotonic; Hyper: Hypertonic (600 mOsm). When the difference reached statistical significance this is indicated with ****P < .01**, *****P < .001**, the number of independent experiments is shown above

turnover rate generated by glycolysis. A classical value for the ATP/O ratio for mitochondrial oxidative phosphorylation is 2.5. If dioxygen (O₂) is considered for OCR, then the ATP/O₂ ratio would be 5. Hence, PPR was compared to five times OCR (Figure 5E,F).

Repression of cellular respiration (OCR) in the presence of glucose was observed and persisted for hours (Figure 5A,E). In addition, we observed an abrupt, but transient, increase in the extracellular acidification rate (Figure 5C,E). Glucose and lactate measurements were attempted in a kinetic experiment with cells in suspension (Supplemental Figure S5). Although rates measurements were not attempted, the values for glucose and lactate concentrations were consistent with higher glucose uptake and lactate release under hyperosmotic conditions. In the absence of glucose, PPR decreased uniformly to about 25% of the glucose value (Compare Figure 5D,F with 5C,E) and OCR was preserved under hyperosmotic conditions (Figure 5B,F). The same results were obtained when glucose was replaced by galactose (Supplemental Figure S6). When HT29 cells were studied following the same protocol, qualitatively similar conclusions were reached (Supplemental Figure S7). At the end of these experiments, a significant number of dead cells were observed in wells subjected to hypertonic conditions. We therefore evaluated cellular viability over time with the neutral red procedure (Figure 6). This confirmed that the hypertonic conditions are deleterious for cellular survival. Interestingly, we observed better preservation of cell viability in absence of glucose (Figure 6B) than in its presence (Figure 6A).

A specific experiment was designed to show, in the short term, how hyperosmotic conditions and glucose contribute to the repression of OCR (Figure 7). In isotonic conditions, the addition of glucose had a modest effect on cellular respiration (Figure 7A). The procedure for mannitol addition first required opening the chamber which re-oxygenated the medium that

led, within seconds, to negative OCR values, and second, dissolution of mannitol which was expected to impact temperature and oxygen solubility. However, after several minutes, a new steady state of oxygen consumption rate was observed, with a slightly lower value than that recorded before mannitol addition (See also Supplemental Figures S2 and S5). This decrease was consistent with the first data points after mannitol addition in the Seahorse (Figure 5B), although two different modes of mannitol addition were used (see Methods section). Subsequently, the addition of glucose caused an immediate further decrease in OCR of much larger amplitude than the same glucose addition in isotonic conditions. For a better comparison, the overlay is shown (Supplemental Figure S8). This decrease appeared proportional to the glucose load in the physiological range (Figure 7B).

3.3 | Decreased cellular ATP turnover rates

The “ATP turnover rates” (Figure 5 and Supplemental Figures S6, S7) are overestimated because the calculation (5 × OCR) was based on the assumption that 100% of OCR is convertible into ATP rate. This is inexact because of the contribution of the leak to the basal OCR. Similarly, the PPR rate would to a certain extent reveal other processes than lactate release. The use of different inhibitors could be used to determine these ATP turnover fluxes during Seahorse experiments.²⁰ However, this would have interrupted the long-term follow-up of cellular respiration under hyperosmotic stress, as shown here (Figure 5, Supplemental Figures S6, S7). We therefore propose a calculation based on data presented here. For the glycolytic ATP turnover, we subtracted the PPR obtained in absence of glucose (values in Figure 5C minus values in Figure 5D). For the OxPhos ATP, we used the short-term experiments (Figure 2) to estimate the fraction

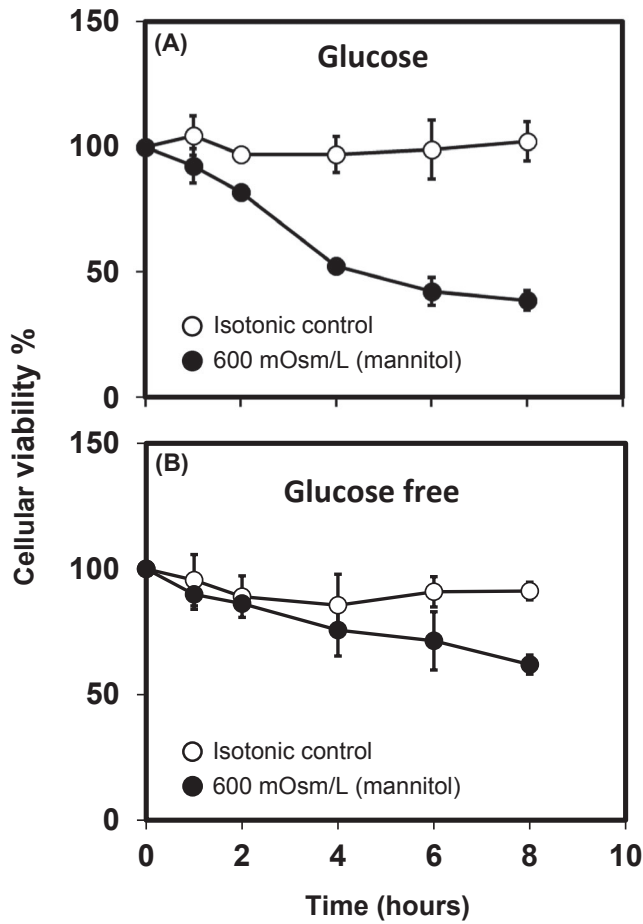


FIGURE 6 Cellular viability. The neutral red cellular uptake was measured after incubation for period of times ranging from zero to eight hours (X-axis) in isotonic (empty circles) or hypertonic (black dots) medium in the presence (A) or absence of glucose (B). The cellular viability was expressed relative to the value for neutral red uptake at time zero in the same medium as the 100% reference. In one experiment, each value is the average from 12 readings (12 wells). The values shown here are the mean values \pm min-max for the two independent experiments

of basal OCR that was actually dedicated to oxidative phosphorylation, which was determined with CHO cells in presence/absence of glucose (Supplemental Figure 4). This value was then used to correct the theoretical yield of oxidative phosphorylation when NADH or FADH₂ coenzymes are re-oxidized by the mitochondrial respiratory chain²¹ and the resulting ATP/O₂ ratio of the complete oxidative pathway was calculated with the assumption that only one type of substrate (glucose or acetyl-CoA) was fully oxidized (Supplemental Figure S10). The OCR was multiplied by this ATP/O₂ ratio to estimate the ATP turnover rate associated to the oxidative pathway. The calculation for total cellular ATP turnover rates in CHO cells is shown with and without these corrections (Figure 8). The hypertonic conditions, independently of the presence/absence of glucose, significantly degraded the

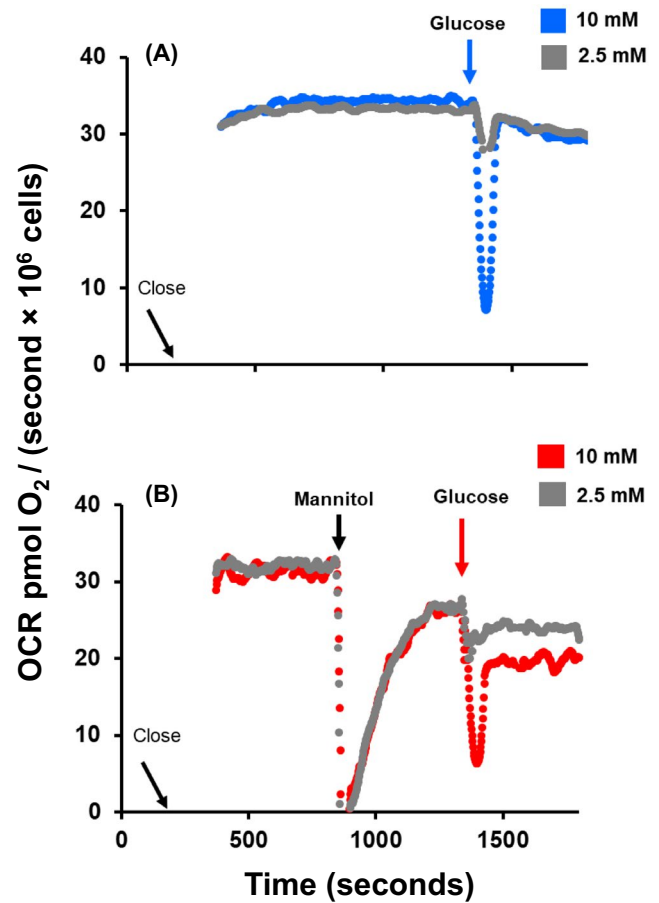


FIGURE 7 Repression of OCR by mannitol and glucose in the short term. X-axis time in second, Y-axis OCR in pmol O₂/ (second \times 10⁶ cells), A and B paired experiments in the O₂k with a same suspension of CHO cells in a DMEM medium without glucose, “Close”: closure of chambers to initiate rates measurement values and the rise to a stable value (>30) representing basal cellular OCR is not shown. Glucose is added simultaneously in each chamber at two different final concentrations: 2.5 mM (grey) or 10 mM (blue/red). A, Additions of glucose in isotonic medium. B, Hypertonic conditions (600 mOsm) with mannitol added first (300 mM same procedure as in Figure 1A) followed by glucose additions. The time needed to restore a new stable oxygen consumption rate after mannitol addition (see legend of Figure 1) could be evaluated with greater accuracy in this graph. A direct comparison (overlay) of the blue and red trace is provided (Supplemental Figure S8)

contribution of OxPhos to cellular ATP turnover. This could not be explained by cell death in the short term (<2 hours) of the experiments. Moreover, Figure 6 suggests that cellular ATP turnover rate and survival were dissociated during this period. The nearly normal basal OCR observed in absence of glucose over approximately 2 hours after osmotic shock (Figure 5B) is, therefore, thought to obscure considerable disruption of cellular bioenergetics (Figure 3, Supplemental Figure S2).

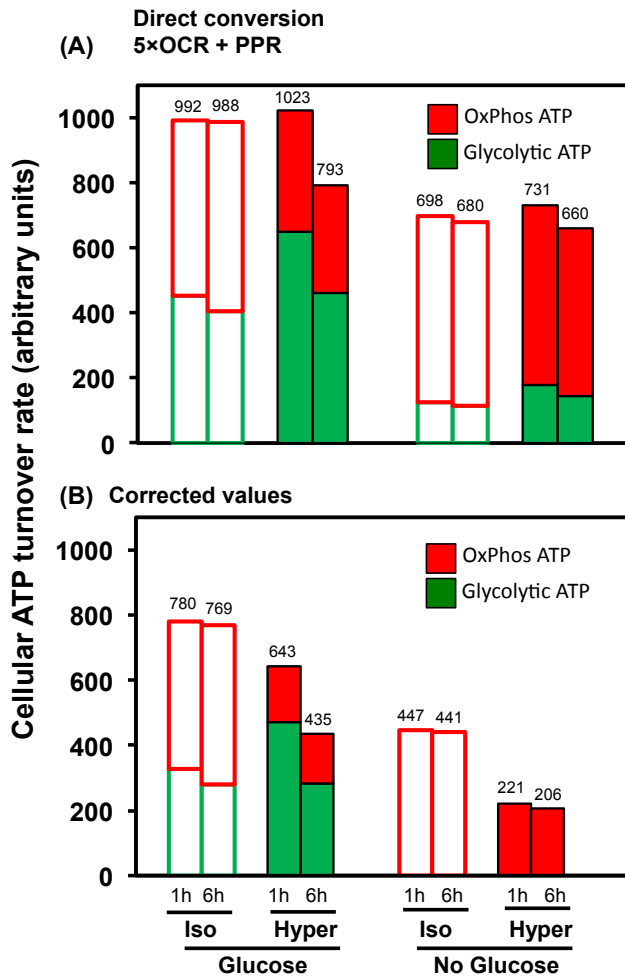


FIGURE 8 Cellular ATP turnover in CHO cells. The Glycolytic ATP (green) and OxPhos ATP (red) turnover rates are summed to evaluate the total cellular ATP turnover rate, this value is indicated above. Empty bars refer to isotonic control and filled bars to hypertonic conditions. A, Uncorrected values, there are the sums of rates as shown in Figure 5E,F. B, Corrected values, the non-glycolytic acidification rate is considered: glycolytic ATP turnover rate = (PPR – PPR no glucose). For the respiratory ATP turnover, the metabolic pathway and the percentage of OCR actually explained by OxPhos (Supplemental Figure S4) are considered to calculate the ATP/O₂ ratio to be applied to each situation (Supplemental Figure 10), then respiratory ATP turnover rate = OCR × ATP/O₂

4 | DISCUSSION

4.1 | Hyperosmolarity impacts mitochondrial oxidative phosphorylation

Cellular ATP consumption is compensated by continuous ATP regeneration, which results from the joint action of glycolysis and respiration. Respiration could be considered as two steps: (i) oxidation (release of CO₂ and oxygen consumption) that releases energy and (ii) use of this energy,

which feeds both oxidative phosphorylation and an inevitable energy loss (leak). Hence, cellular ATP demand stimulates oxidation above the leak value. Similarly, uncoupler (CCCP) stimulates oxygen consumption to a maximal value (ETS). This ETS is a maximal oxidation rate that places an absolute limitation to the possible increase in ATP regeneration rate. The use of oligomycin allows evaluating both Leak and OxPhos (for more details, see materials and methods section). The OxPhos rate was shown to be the most affected step (Figure 3, Supplemental Figure S4). As the leak was unaffected or increased, the impact on the basal cellular oxygen consumption rate was less (Figure 3, Supplemental Figure S2).

The lowering of ETS indicated an impact on the oxidation step. However, this is unlikely to explain all the effects of hyperosmolarity on cellular respiration. First, this decrease in ETS is dependent on the presence of glucose while the impact of hyperosmolarity on the OxPhos is similar in either the presence or absence of glucose (Figure 3). Moreover, if the maximal oxidation rate constitutes the limiting factor, one would expect the ETS to be roughly equal to basal; while both appeared similarly affected (Figure 3), the ETS remained always higher than the basal (Figure 2, Supplemental Figure S3). In our schematic description of cellular bioenergetics presented above, the two other targets for hyperosmolarity could be either the cellular ATP consumption rate or the OxPhos itself. If the cellular ATP consumption rate would be the target, the recruitment of ATP producing pathways other than OxPhos would not be expected. In contrast, impact on OxPhos would result in imbalance between ATP need and ATP regeneration. This ought to be compensated for by other ATP generating pathways and/or to negatively impact cellular viability, two consequences observed in our study. Therefore, osmolarity is likely to target OxPhos in first instance. However, this could not be reproduced/confirmed by the mere exposure of isolated mitochondria to hypertonic conditions (Figure 4).

4.2 | Bioenergetic adaptative strategies under hyperosmotic conditions

The detrimental effect of hypertonic condition on respiration induces cellular responses. If glucose is available, it could produce a large increase in glycolytic rate with lactate release (Figures 5, 8, Supplemental Figures S5, S7). However, strategies alternative to lactic fermentation are to be considered to explain cell survival for hours in absence of glucose (Figures 5, 6). Mitochondrial oxidation of substrates releases ATP via two different enzymatic activities: the mitochondrial complex V of the OxPhos pathway (the target of the inhibitor oligomycin) and the oxidation of Acetyl-CoA into CO₂ by the Krebs cycle, which includes

a step of substrate linked phosphorylation. The distinction between the two is usually ignored because both are ultimately dependent on the re-oxidation of NADH produced by the Krebs cycle at the level of the mitochondrial respiratory chain. However, in the context of impaired OxPhos, the role of the leak should be considered. Increasing the leak would promote NADH re-oxidation and, hence, would accelerate the substrate-linked phosphorylation step. This process would cause complete oxidation of glucose (CO₂ release), uncoupled mitochondrial respiration, and would release four ATP per glucose; twice as much as the glucose to lactate pathway. More importantly, this phosphorylation step could take place with any substrate susceptible to be engaged in the Krebs cycle, such as acetyl CoA (hence fatty acid oxidation) or amino acids (notably glutamine). Therefore, the greatest increase in leak observed in the absence of glucose (Figure 3) could be interpreted as the mitochondrial adaptive response to enhance this ATP production process independent from OxPhos and glucose.

The calculation of the ATP turnover rate under hyperosmotic conditions in the absence of glucose showed a reduction to half of its value under isotonic conditions (Figure 8). A decrease in cellular ATP turnover in critical situations during which cell survival becomes dependent on a drastic reduction of ATP use with re-orientation to vital functions is well documented.²²⁻²⁴ Given the poor yield of non-OxPhos pathways of ATP production, it constitutes by far the most effective adaptive strategy to compensate for a decrease in OxPhos. Therefore, while hypometabolism seems unlikely to represent the primary event caused by hyperosmotic conditions it ought to be induced for cell survival. We summarize the remodeling of cellular energy metabolism shown here in presence/absence of glucose in Figure 9. For the sake of simplicity, the effect of hyperosmotic conditions is assumed to be the reduced activity of mitochondrial complex V revealed by use of oligomycin in this study. It must be emphasized here that this observation does not prove that complex V is the target of hyperosmotic conditions. Therefore, the pathways by which hyperosmolarity causes decrease in OxPhos and reduces ATP turnover rate remain to be explored.

4.3 | Hyperosmolarity enhances the Warburg/Crabtree effect

The present study showed that hyperosmotic conditions greatly aggravated the deleterious effect of glucose on the basal respiratory rate (Figures 3, 5, and 7). This effect is known as the “Warburg” or “Crabtree” effect depending on the system considered (mammalian cells or yeast). This inhibition of respiration by glucose in the short term has

been well studied in yeast (Crabtree effect),²⁵ although the molecular mechanisms are still under debate but exclude time-consuming processes such as changes in gene/protein expression. The proposed explanations are either a direct competition between glycolysis and respiration for common metabolic intermediates (ADP, Phosphate) or the inhibition of respiration by intracellular messengers.²⁶ There are several candidates such as calcium²⁷ and/or intermediates of glycolysis (notably fructose 1-6 biphosphate), which have been shown to inhibit mitochondrial respiration at the level of complexes III and IV.²⁸ This would better fit with our results than competition for ADP or Pi as the effect is still present when the oxidation rate is independent from ADP phosphorylation (ETS rate Figures 2, 3, Supplemental Figure S2). These mediators could be considered as diffusible molecules and therefore the permeabilization of cells would lead to their dilution in a much larger volume. Consequently, when the inhibition had been primed with glucose, it was expected to disappear after permeabilization. Initial experiments failed to confirm this (Supplemental Figure S9). Other explanations might be pertinent for the mechanisms underlying the Crabtree effect but they are beyond the scope of this study and were not investigated further. In conclusion, a two-step model could be proposed (Figure 9B). First, hyperosmolarity impairs OxPhos. The increased recourse to glycolysis is at the origin of the second hit: the Warburg/Crabtree effect. This takes place within a time frame of, at most, few minutes and possibly seconds (Figures 5, 7, Supplemental Figures S2, S5, S7, S9).

The balance (competition) between glycolysis and respiration is a long debated issue pertinent to cancer and inflammation (see introduction). This is usually considered within a time scale compatible with long-term changes implying, for example, modifications of gene expression and rewiring of metabolism toward a cellular program such as cellular proliferation in the case of cancer.^{11,29-32} One of the earliest event of the inflammatory reaction is the vascular response that takes place within few minutes^{33,34} and is expected to increase osmotic pressure at the inflammatory site. Therefore, this study raises the issue that to some extent the metabolic shift toward glycolysis associated with inflammation may result from this fast metabolic response to hyperosmotic conditions. This effect could be exerted on incoming immune cells independently of (or potentiating) the action of specific inflammation mediators.

Beside the determination of the exact mechanism by which hyperosmolarity triggers the changes observed here, two other issues deserve consideration: (i) could the phenomenon observed here constitute a priming event for a remodeling of cellular metabolism that would persist over time and even if conditions return to normal? (ii) is this metabolic

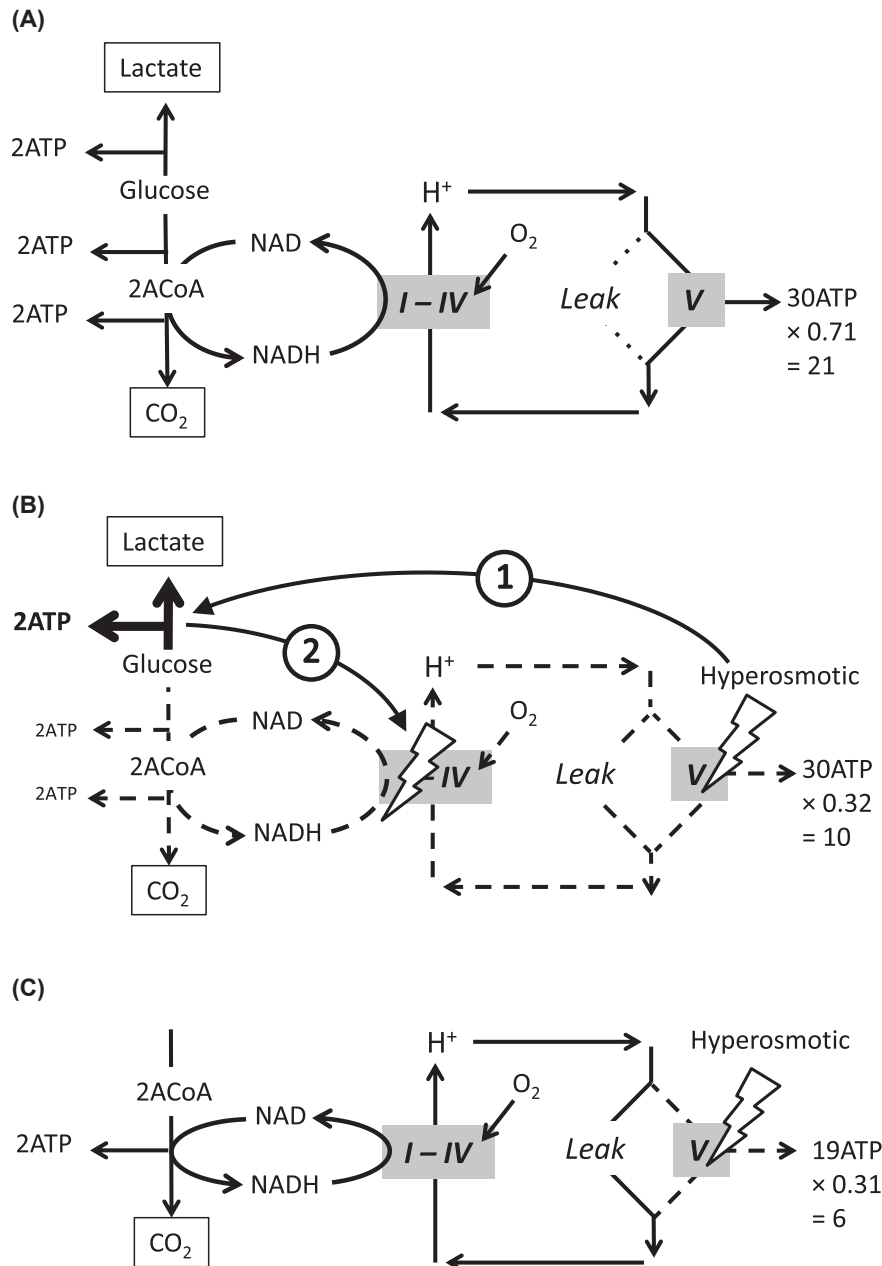


FIGURE 9 Cellular ATP production circuits. The schemes A, B refer to a situation in which glucose would be the sole substrate. ATP is produced by two pathways: glycolysis that produces two ATP per glucose and releases two lactates or complete oxidation by which glucose is converted into the intermediate Acetyl-CoA (ACoA) whose oxidation into CO₂ release one ATP (two ACoA and ATP per glucose oxidized). This is accompanied by reduction of coenzymes (figured as NAD/NADH only for the sake of simplicity), their re-oxidation by the mitochondrial respiratory chain redox complexes (I-IV) generates a proton gradient (H⁺) across the mitochondrial inner membrane. Use of this proton gradient is shared between ATP production by mitochondrial complex V and leak. The values of 2.7 and 1.6 for the number of ATP formed from NADH or FADH₂, respectively,²¹ lead to a value of 30.2 of OxPhos ATP per glucose (shown here as 30). This theoretical value corresponds to a situation in which 100% of coenzyme re-oxidation contributes to ATP formation. This is inexact because of the leak and of non-mitochondrial coenzymes re-oxidation. The determination of the fraction of the cellular OCR dedicated to ATP formation (bold values in Supplemental Figure S4) is used to estimate more realistic values for the OxPhos ATP. A, Isotonic conditions, the theoretical value of 30 ATP/glucose for the OxPhos is lowered to 21. B, C, Hyperosmotic conditions, for the sake of simplicity the effect of hyperosmolarity is figured as the inhibition of complex V although there is no proof for such a direct action (see text). B, In the presence of glucose, the decreased activity of complex V would cause glycolytic compensation (curved arrow 1) and the increased glycolytic rate results in the Crabtree effect with inhibition of mitochondrial redox complexes (curved arrow 2). C, In the absence of glucose, the oxidation of two molecules of acetyl-CoA is considered. The reduced activity of complex V has the supplementary consequence to impair the oxidation of acetyl-CoA because it is dependent on the re-oxidation of coenzymes. Increase in Leak restores OCR and re-oxidation of coenzymes, hence increases the contribution of acetyl-CoA oxidation to ATP production

response specific to hyperosmotic conditions or does it reflect the earliest response to a wide range of cellular stress? Answers to these two questions may alter our understanding of the metabolic conversion of cells such as observed in inflammation and cancer.

ACKNOWLEDGMENTS

The authors wish to thank Inserm, CNRS, and Université Paris Descartes (now Université de Paris) for support and Dr Ken Olson for reading/editing the manuscript.

CONFLICT OF INTEREST

The authors declare no conflict of interest.

AUTHORS CONTRIBUTIONS

L. Schwartz, R. Abolhassani, and F. Bouillaud designed research; M. Hamraz performed experiments with help of C. Ransy and V. Lenoir. M Andriamihaja contributed new reagent; M. Hamraz and F. Bouillaud analyzed the data; M. Hamraz, L. Schwartz, and F. Bouillaud wrote the paper.

REFERENCES

1. Brocker C, Thompson DC, Vasiliou V. The role of hyperosmotic stress in inflammation and disease. *BioMol Concepts*. 2012;3(4):345-364.
2. Schilli R, Breuer RI, Klein F, et al. Comparison of the composition of faecal fluid in Crohn's disease and ulcerative colitis. *Gut*. 1982;23(4):326-332.
3. Schwartz L, Guais A, Pooya M, Abolhassani M. Is inflammation a consequence of extracellular hyperosmolarity? *J Inflamm*. 2009;6(1):21.
4. Light RW, Macgregor MI, Luchsinger PC, Ball WC. Pleural effusions: the diagnostic separation of transudates and exudates. *Ann Intern Med*. 1972;77(4):507-513.
5. Stohrer M, Boucher Y, Stangassinger M, Jain RK. Oncotic pressure in solid tumors is elevated. *Cancer Res*. 2000;60(15):4251-4255.
6. Jain RK, Cook AW, Steele EL. Haemodynamic and transport barriers to the treatment of solid tumours. *Int J Radiat Biol*. 1991;60(1-2):85-100.
7. Di Paolo A, Bocci G. Drug distribution in tumors: mechanisms, role in drug resistance, and methods for modification. *Curr Oncol Rep*. 2007;9(2):109-114.
8. Eales KL, Hollinshead KER, Tennant DA. Hypoxia and metabolic adaptation of cancer cells. *Oncogenesis*. 2016;5(1):e190.
9. Brand MD, Nicholls DG. Assessing mitochondrial dysfunction in cells. *Biochem J*. 2011;435(Pt 2):297-312.
10. Warburg O. On the origin of cancer cells. *Science*. 1956;123(3191):309-314.
11. Koppenol WH, Bounds PL, Dang CV. Otto Warburg's contributions to current concepts of cancer metabolism. *Nat Rev Cancer*. 2011;11(5):325-337.
12. Asgari Y, Zabihinpour Z, Salehzadeh-Yazdi A, Schreiber F, Masoudi-Nejad A. Alterations in cancer cell metabolism: the Warburg effect and metabolic adaptation. *Genomics*. 2015;105(5):275-281.
13. Heiden MG, Cantley LC, Thompson CB. Understanding the Warburg effect: the metabolic requirements of cell proliferation. *Science*. 2009;324(5930):1029-1033.
14. Moreira J, Hamraz M, Abolhassani M, et al. The Redox status of cancer cells supports mechanisms behind the Warburg effect. *Metabolites*. 2016;6(4):33.
15. Liu TF, Brown CM, El Gazzar M, et al. Fueling the flame: bioenergy couples metabolism and inflammation. *J Leukoc Biol*. 2012;92(3):499-507.
16. Hotamisligil GS. Inflammation, metaflammation and immunometabolic disorders. *Nature*. 2017;542(7640):177-185.
17. El Kasmi KC, Stenmark KR. Contribution of metabolic reprogramming to macrophage plasticity and function. *Semin Immunol*. 2015;27(4):267-275.
18. Zweibaum A, Pinto M, Chevalier G, et al. Enterocytic differentiation of a subpopulation of the human colon tumor cell line HT-29 selected for growth in sugar-free medium and its inhibition by glucose. *J Cell Physiol*. 1985;122(1):21-29.
19. Repetto G, del Peso A, Zurita JL. Neutral red uptake assay for the estimation of cell viability/cytotoxicity. *Nat Protoc*. 2008;3(7):1125-1131.
20. Seahorse XF Real-Time ATP Rate Assay Kit|Agilent. [Online]. <https://www.agilent.com/en/products/cell-analysis/seahorse-xf-consumables/kits-reagents-media/seahorse-xf-real-time-atp-rate-assay-kit#howitworks>. Accessed June 26, 2019.
21. Watt IN, Montgomery MG, Runswick MJ, Leslie AGW, Walker JE. Bioenergetic cost of making an adenosine triphosphate molecule in animal mitochondria. *Proc Natl Acad Sci*. 2010;107(39):16823.
22. Hochachka PW, Lutz PL. Mechanism, origin, and evolution of anoxia tolerance in animals. *Comp Biochem Physiol B Biochem Mol Biol*. 2001;130(4):435-459.
23. Buck LT, Pamerter ME. Adaptive responses of vertebrate neurons to anoxia—matching supply to demand. *Respir Physiol Neurobiol*. 2006;154(1-2):226-240.
24. Boutilier RG. Mechanisms of cell survival in hypoxia and hypothermia. *J Exp Biol*. 2001;204(Pt 18):3171-3181.
25. Crabtree HG. Observations on the carbohydrate metabolism of tumours. *Biochem J*. 1929;23(3):536-545.
26. Rosas Lemus M, Roussarie E, Hammad N, et al. The role of glycolysis-derived hexose phosphates in the induction of the Crabtree effect. *J Biol Chem*. 2018;293(33):12843-12854.
27. Wojtczak L, Teplova VV, Bogucka K, et al. Effect of glucose and deoxyglucose on the redistribution of calcium in ehrlich ascites tumour and Zajdela hepatoma cells and its consequences for mitochondrial energetics. Further arguments for the role of Ca(2+) in the mechanism of the crabtree effect. *Eur J Biochem*. 1999;263(2):495-501.
28. Díaz-Ruiz R, Avéret N, Araiza D, et al. Mitochondrial oxidative phosphorylation is regulated by fructose 1,6-bisphosphate. A possible role in Crabtree effect induction? *J Biol Chem*. 2008;283(40):26948-26955.
29. Warburg O, Wind F, Negelein E. The metabolism of tumors in the body. *J Gen Physiol*. 1927;8(6):519-530.
30. Hanahan D, Weinberg RA. Hallmarks of cancer: the next generation. *Cell*. 2011;144(5):646-674.
31. DeBerardinis RJ, Chandel NS. Fundamentals of cancer metabolism. *Sci Adv*. 2016;2(5):e1600200.
32. Gaude E, Frezza C. Tissue-specific and convergent metabolic transformation of cancer correlates with metastatic potential and patient survival. *Nat Commun*. 2016;7:1-9.

33. Wedmore CV, Williams TJ. Control of vascular permeability by polymorphonuclear leukocytes in inflammation. *Nature*. 1981;289: 646-650.
34. Acute Inflammation. [Online]. <https://courses.washington.edu/conj/inflammation/acuteinflam.htm>. Accessed November 7, 2018.

SUPPORTING INFORMATION

Additional supporting information may be found online in the Supporting Information section.

How to cite this article: Hamraz M, Abolhassani R, Andriamihaja M, et al. Hypertonic external medium represses cellular respiration and promotes Warburg/Crabtree effect. *The FASEB Journal*. 2019;00:1–15. <https://doi.org/10.1096/fj.201900706RR>